Projected Response of Low-Level Convergence and Associated Precipitation to Greenhouse Warming

Article *in* Geophysical Research Letters · October 2017
DOI: 10.1002/2017GL075489

3 authors, including:

Evan Weller
Monash University (Australia)
31 PUBLICATIONS **450** CITATIONS
SEE PROFILE

Christian Jakob
Monash University (Australia)
162 PUBLICATIONS **4,445** CITATIONS
SEE PROFILE

Projected response of low-level convergence and associated precipitation to greenhouse warming

Evan Weller[1,2]*, Christian Jakob[1,2], and Michael J. Reeder[1,2]

[1]School of Earth, Atmosphere and Environment, Monash University, Victoria, Australia

[2]Centre of Excellence for Climate System Science, Monash University, Victoria, Australia

Revision submitted to *Geophys. Res. Lett* (2017-9-27)

* Corresponding author:

Evan Weller

School of Earth, Atmosphere and Environment, Monash University, 9 Rainforest Walk, Monash University, Victoria, 3800, Australia.

E-mail: evan.weller@monash.edu

This article has been accepted for publication and undergone full peer review but has not been through the copyediting, typesetting, pagination and proofreading process which may lead to differences between this version and the Version of Record. Please cite this article as doi: 10.1002/2017GL075489

Abstract

The parameterization of convection in climate models is a large source of uncertainty in projecting future precipitation changes. Here, an objective method to identify organized low-level convergence lines has been used to better understand how atmospheric convection is organized and projected to change, as low-level convergence plays an important role in the processes leading to precipitation. The frequency and strength of convergence lines over both ocean and land in current climate simulations is too low compared to reanalysis data. Projections show a further reduction in the frequency and strength of convergence lines over the mid-latitudes. In the tropics, the largest changes in frequency are generally associated with shifts in major low-latitude convergence zones, consistent with changes in the precipitation. Further, examining convergence lines when in the presence or absence of precipitation results in large spatial contrasts, providing a better understanding of regional changes in terms of thermodynamic and dynamic effects.

1. Introduction

The hydrological cycle is, perhaps, the most important aspect of Earth's climate, and consequently any change in its variability is of great social, economic and scientific importance. However, predicting the availability of water or lack thereof, and its sometimes-devastating effects via floods and droughts, remains a major scientific challenge in weather and climate research. This challenge is due, in large measure, to the difficulty in predicting the occurrence and intensity of precipitation.

Almost all precipitation is associated with upward motion in the atmosphere, which is the result of the internal circulations of weather systems (Birch *et al*., 2014; Bony *et al*., 2015). Tied to this upward motion, organized convergence of mass in the boundary layer sometimes triggers and organizes precipitation, while the associated moisture flux provides the water necessary for sustained precipitation (Reeder *et al*., 2013; Birch *et al*., 2014; Birch *et al*., 2015). For example, the regions of highest precipitation coincide with the regions of long-lived large-scale convergence, such as the Inter-Tropical Convergence Zone (ITCZ) and the South Pacific Convergence Zone (SPCZ) (Hastenrath, 1995; Widlansky *et al*., 2010; Berry and Reeder, 2014; Wodzicki and Rapp, 2016).

One necessary condition for a climate model to be judged an accurate representation of the Earth system is that it not only reproduces the correct statistical properties of rainfall, but that it does so for the right physical reasons. In other words, evaluating the performance of a climate model must include an evaluation of how well the model represents the dynamical process responsible for precipitation. One such important dynamical process is the triggering and organization of precipitation by long-lived large-scale convergence lines. Moreover, as the cloud processes that ultimately produce precipitation occur on small scales, the need to parameterize them in climate models is generally thought to be one of the biggest sources of

uncertainty in climate model projections (e.g., Jakob, 2014; Rybka and Tost, 2014). Nonetheless, climate models are designed to simulate the main large-scale circulations leading to precipitation (or its suppression). Therefore, examining these components prior to the conceptual parameterizations for representing clouds and microphysical processes can provide some confidence in the simulated precipitation and its future changes (Shepherd, 2014).

It is thought that increases in the specific humidity in a warmer world and the associated changes in the moisture transport will intensify the precipitation in those regions in which the precipitation is currently high. This mechanism for increased precipitation has commonly been termed as the 'wet-get-wetter' mechanism, or the thermodynamical component in precipitation change (Held and Soden, 2006; Chou *et al*., 2009; Seager *et al*., 2010; Chadwick *et al*., 2013; Kent *et al*., 2015; Wills *et al*., 2016). However, it has been shown that this mechanism does not dominate the overall spatial pattern of precipitation change, at least in the tropical regions (Chadwick *et al*., 2013; Kent *et al*., 2015). Instead, Chadwick *et al*. (2013) and Kent *et al*. (2015) for example, find that there is a large cancellation over much of the tropical oceans between the spatial patterns of thermodynamic and divergence feedback components in future precipitation changes. This cancellation results in the spatial pattern of precipitation change being largely determined by the dynamical component associated with spatial shifts in convective mass flux. This dynamical component dominates both the pattern of climate model ensemble mean precipitation change and the inter-model uncertainty in the pattern. Much of the dynamical change in precipitation in the tropics is consistent with the pattern of spatial change in low-level convergence and convection, which may be driven by several mechanisms such as sea surface temperature (SST) gradient changes, land-sea temperature contrast changes, and local changes in atmosphere circulation. In general, over the oceans the pattern of spatial mass-flux change is consistent with the hypothesis that SST pattern changes play the dominant

role in determining changes in the position of low-level convergence and convection (Xie *et al*., 2010; Chadwick *et al*., 2013; Huang *et al*., 2013; Kent *et al*., 2015).

A large percentage of precipitation (up to 90%) over the tropical and subtropical latitudes has been shown to be associated with organized low-level convergence lines (Weller *et al*., 2017). Therefore, it is likely that convergence lines are an important dynamical component of future precipitation changes. The current study objectively identifies convergence lines in models in the Coupled Model Intercomparison Project Phase 5 (CMIP5; Taylor *et al*., 2012), the aims being to better understand: how these precipitation-producing convergence lines, and areas of atmospheric convection more generally, are organized on scales resolved by the models; and how precipitation-producing convergence lines are projected to change in warmer world. The main result of the work is that, because of the strong dynamical relationship between organized convergence and precipitation, changes in the objectively identified convergence lines qualitatively account for most of what has been broadly termed the dynamical component of precipitation changes in earlier studies.

2. Method and data

Wind fields from climate models and reanalyses are examined using the objective instantaneous convergence line identification method described in detail by Weller *et al*. (2017), which is a modified version of that developed by Berry and Reeder (2014). In brief, convergence line points are identified as locations of minima in the divergence field, and a line joining algorithm is used to link the points into organized convergence lines. In the current study, the method is applied to 6-hourly divergence fields calculated at 850 hPa. In previous studies (e.g., Weller *et al*. 2017) a divergence threshold of -1×10^{-6} was used to identify regions

of convergence. Here, we set the minimum divergence threshold to zero, i.e., we include all regions of convergence in the identification method. We make this choice in order to avoid any influence on model evaluation that may be due to setting such a threshold when comparing numerous climate model and reanalysis data sets, or different climate scenarios. We also do not apply any minimum line length threshold, but note that at least two points are required for a convergence line to be identified.

In a second important step, precipitation is associated with the objectively identified convergence lines when they are found to be close to each other for each 6-hourly field (see Weller *et al*. (2017) for details). In the current study, adjacent grid points (±1 grid point in size) are searched for an identified convergence line for each rain grid point to account for all the precipitation that may be related to the broader system associated with a convergence line. The 6-hourly times are then aggregated to determine how much of the daily precipitation is associated with organized convergence at each grid point.

The Interim European Centre for Medium-Range Weather Forecasts (ECMWF) Re-Analysis (ERA-Interim; Dee *et al*. 2011) and the National Oceanic and Atmospheric Administration (NOAA)/Climate Prediction Center (CPC) morphing technique (CMORPH; Joyce *et al*. 2004) data sets are used to calculate an observationally constrained atlas of convergence lines and associated precipitation against which to evaluate the model data. Here ERA-Interim wind fields at 1.5° horizontal resolution for the period 1979-2005 are analyzed. The same objective convergence line identification method is applied to 10 CMIP5 models (listed in Table 1 of the Supplementary Information). The models were chosen from the complete set participating in CMIP5 based on the availability of the required 6-hourly data from both current and future climate simulations. Simulations incorporating historical anthropogenic forcing (greenhouse gases, aerosols, and other anthropogenic forcing agents) and natural forcing (solar and volcanic

activities) for the period 1979-2005 are used to evaluate the representation of convergence lines in the current climate. Simulations incorporating future greenhouse gases and aerosols under the emission scenario of Representative Concentration Pathway 8.5 (RCP8.5) for the period 2080-2099 are used to examine future changes in organized convergence lines and associated precipitation towards the end of the 21st century. Model wind and precipitation data are interpolated onto the same 1.5° horizontal grid as the ERA-Interim data prior to calculating the divergence, identifying the convergence lines, and calculating the proportion of precipitation associated with these convergence lines. In all figures that show spatial maps, regions where the surface topography is higher than 850 hPa, and which were therefore not analyzed, are shaded gray.

3. Current climate simulations

The annual-mean frequency of instantaneous convergence lines is shown in Figure 1, expressed as the proportion of month (% month^{-1}), for ERA-Interim (Figure 1a) and the multimodel mean of the historical simulations (Figure 1b). Overall, the pattern of convergence line occurrence in the multimodel mean is consistent with ERA-Interim with the largest values within the major ITCZs of all three ocean basins, and over land in tropical monsoonal regions of Africa, India and South America. The models also simulate high frequencies of occurrence in the mid-latitudes at approximately 40° over the oceans, and the lowest values (less than 5%) on the eastern flank of the subtropical highs, consistent with the observations. However, the models generally simulate too few convergence lines, as highlighted in Figure 1c by the difference between the multimodel mean and ERA-Interim. The largest bias is over the tropical oceans and is about 10%, decreasing poleward in both hemispheres. The tropical regions where large biases occur also exhibit a larger standard deviation in convergence line occurrence throughout

the year, whereas most land regions exhibit reduced variability compared to observations (Supplementary Figure 1a-c).

The mean strength of the convergence lines is shown in Figures 1d-1f for ERA-Interim, the multimodel mean for the historical simulation, and the difference (multimodel mean minus ERA-Interim), respectively. The strength of the convergence lines from the multimodel mean is simulated well in high precipitation regions across the tropics and within the major convergence zones. However, the strength is relatively weak in low precipitation regions, particularly poleward of 20°, where large negative biases (about 0.25 x 10^{-5} s^{-1}) are found over the mid-latitude storm tracks, northern Africa and southern South America. Conversely, the strength of the convergence lines over some land regions with high precipitation (i.e. northern South America and parts of equatorial Africa) is overestimated (about 0.3 x 10^{-5} s^{-1}). The variability in the strength of the convergence lines also exhibits a similar pattern of slightly larger variability over low-latitudes and less variability over mid-latitudes (Supplementary Figure 1d-f).

4. Role of convergence lines in future precipitation change

The annual-mean frequency map of instantaneous convergence lines for the multimodel mean RCP8.5 simulation is shown in Figure 2a, and the change compared to the historical simulation is shown in Figure 2b. Although the overall structure of the current climate appears to remain, there are consistent changes across all models, especially in the oceanic regions. Over the central Indian Ocean there is a decrease immediately south of the equator as well as in a zonal band centered at 40°S and an increase over the remaining Indian Ocean. Over the Pacific Ocean there is a shift in the pattern of convergence lines towards the equator in the east and a slight

increase in the North Pacific at 20°N. The shifted pattern of change and the reduction in the frequency in the Southern Hemisphere Pacific Ocean suggests a more zonal and less organized SPCZ. Models from both CMIP5 and the earlier CMIP3 that simulate the SPCZ well show a consistent tendency towards a more zonally oriented SPCZ in the future (Cai *et al*., 2012b). The mechanism appears to be associated with a reduction in near-equatorial meridional SST gradients, which is a robust feature of the modeled SST response to anthropogenic forcing (Widlansky *et al*., 2013). In the Atlantic Ocean the pattern of convergence lines shifts from north of the equator to the south, and decreases over the mid-latitudes. The associated convergence line strength (Figure 2c) and its change in magnitude (Figure 2d) for the RCP8.5 simulations show that frequency changes are mostly associated with a reduction in the strength of convergence lines. This result is important as the models generally underestimate the strength of the convergence lines in current climate simulations. However, this reduction in strength of convergence lines in regions of high precipitation such as the tropical oceans and the global land monsoon regions is consistent with a reduction in the mean convergence shown by past studies (Held and Soden, 2006; Vecchi and Soden, 2007; Christensen *et al*., 2013; Kjellsson, 2015) despite an overall increase in precipitation over those regions. The reduction in the strength of the convergence arises due to a weakening of the tropical circulation under global warming associated with lower-troposphere water vapour increases and changes to the static stability of the atmosphere. There is a slight increase in the magnitude of the convergence lines in the eastern tropical Pacific in association with the increased frequency. The largest decrease in the strength of convergence lines is co-located with large reductions in the frequency of convergence lines in the mid-latitudes, also consistent with warming-related reductions in the large-scale circulation and a poleward expansion of subtropical dry zones (Lu *et al*., 2007; Seager *et al*., 2010; Scheff and Frierson, 2011).

The above results relate to the annual mean changes. Figure 3 shows the zonal mean seasonal change in the simulated frequency of convergence lines. In the current climate, the multimodel mean simulates well the shift in both the maximum in frequency of convergence lines (shading) and precipitation (solid contours) from the Southern Hemisphere to the Northern Hemisphere in their respective summers compared to observations (Figure 3a,b). The shift in the maximum in the precipitation to the Northern Hemisphere around April-May is delayed by about one month in the multimodel mean. The future seasonal frequency changes of convergence lines show a weakening of the seasonal cycle around the equator, with opposing anomalies straddling each side (Figure 3c). Overall, a slightly more symmetrical response appears to emerge in low-latitudes. The decrease at 40°S in the southern mid-latitudes in the annual mean pattern (Figure 2b) decreases throughout the entire year. Over similar Northern Hemisphere latitudes, there is a slight increase in convergence line frequency during the summer months, suggestive of an increase in the amplitude of the seasonal cycle.

Over the tropical oceans, precipitation changes are presumably associated with the change in SST under further greenhouse warming in future climate simulations (Huang *et al*., 2013). This leads to a different precipitation change pattern from that simply due to changes in the climatological convergence zones, especially for the annual mean shown in Figure 2b. Figure 4a shows the multimodel mean projected change in precipitation and SST by the end of the 21st century. Note that the color scale in Figure 4 is opposite to that of the previous figures in order to denote decreases in precipitation in red (i.e. drying), and therefore blue represents an increase in precipitation. The most striking change is an increase in both precipitation and SST over the equatorial Pacific, an area with minimal change in the frequency of organized convergence lines, except in the east. However, there are some similarities between future changes in precipitation and that in convergence lines. For example, both convergence lines and precipitation exhibit a band of increase centered at roughly 20°N extending from Africa to the

west Pacific. There are also consistent decreases over the equatorial Indian Ocean and a NW-SE oriented band in the east Pacific (c.f. Figures 2b and 4a).

Projected regional precipitation changes due to changes in the convergence line frequency can be better understood by examining the precipitation change that is associated solely with convergence lines. This is since changes in precipitation are simulated to be more regionally variable than changes in temperature, caused by the modulation from regional systems such as the monsoons and tropical convergence zones (Christensen *et al*., 2013). A large fraction of the precipitation (between 65-90%) has been shown to be associated with organized convergence lines using reanalysis and satellite data for many regions across the globe (Weller *et al*., 2017; Supplementary Figure 2a,d). Similarly, large proportions of the simulated precipitation in the models can also be attributed to convergence lines at the sub-daily scale, although in most regions it is about 10-15% less than observed (Supplementary Figure 2e,f). This difference in the precipitation associated with convergence lines indicates that the coupling of precipitation and convergence lines is weaker in the models than in the observations. Moreover, the multimodel mean precipitation is lower over high precipitation regions and higher over low precipitation regions (Supplementary Figure 2a-c). Figure 4b shows the future change in the proportion of precipitation associated with convergence lines. The largest decreases in precipitation over the subtropical eastern Pacific and the equatorial Indian Ocean are regions where the proportion associated with convergence lines also decreases (c.f. Figures 4a and 4b). In contrast, the changes in the subtropical Atlantic Ocean are very different. For example, the multimodel mean projects a small decrease (increase) in precipitation over the Northern (Southern) Hemisphere in the Atlantic, whereas the frequency of convergence lines and the associated precipitation in both hemispheres in the subtropical Atlantic decreases. More so, over the equatorial Atlantic Ocean, precipitation increases (decreases) to the north (south) of the equator, yet the opposite is again seen for the changes in convergence line frequency and

their associated precipitation. These regional changes could be due to opposing contributions from the thermodynamic and dynamical components to the total precipitation change (Bony *et al*., 2013; Chadwick *et al*., 2013; Kent *et al*., 2015; Wills *et al*., 2016), or increases in the horizontal gradient in specific humidity and the resultant increases in dry advection into convergence zones (Neelin *et al*., 2003). Consequently, precipitation may decrease on the flanks of a convergence zone.

To better understand future convergence line frequency changes and how they relate to changes in regional precipitation, we separate cases when a convergence line is associated with precipitation (termed here wet convergence) from those when it is not associated with precipitation (termed here dry convergence). In current climate simulations, convergence lines are associated with precipitation slightly too often compared to observations (Supplementary Figure 3) because the models produce precipitation that is too light too often (Stephens *et al*., 2010). Despite this, the projected changes in dry and wet convergence lines highlight regional differences where thermodynamic changes appear to influence convergence lines and their association with precipitation (Figure 4c,d). For example, over the eastern Pacific the large pattern shift change of convergence lines towards the equator is mainly associated with wet convergence lines, resulting in the decrease in precipitation over the subtropical regions (c.f. Figures 4a and 4d). In contrast, over the equatorial and western Pacific and the SPCZ, there is an increase in wet convergence lines despite little to no change in the overall frequency of organized convergence (c.f. Figures 2b and 4d). This result is consistent with thermodynamic effects predominantly leading to precipitation increases over these regions, hence the frequency of dry convergence lines also decreases (Figure 4c). Conversely, over the equatorial Atlantic, reduced precipitation to the south appears to be due to a projected increased frequency of dry convergence lines (c.f. Figures 2b and 4c). Tied to this is a decrease in wet convergence lines north of the equator in the Atlantic, the two together giving the impression of a spatial shift in

the overall organized convergence (c.f. Figures 2b and 4d), which is opposite to that in precipitation changes. Similar increases in dry convergence line occurrence over land lead to large spatial ocean-land contrasts in the projected changes of convergence lines in the presence or absence of precipitation. This result is consistent with an increased tendency for the convection over land to move and occur more over the ocean under further anthropogenic surface warming (Chadwick *et al*., 2014; He *et al*., 2014; Kent *et al*., 2015).

5. Concluding discussion

Using the objective method of Weller *et al*. (2017), we have identified organized low-level convergence lines in 10 CMIP5 models for which sub-daily data were available. The frequency of occurrence and the strength of the convergence lines in simulations of the current climate were compared with similar calculations with the ERA-Interim reanalysis.

There is reasonable spatial consistency between observations and models in the frequency of convergence lines. However, the convergence lines in the models occur less frequently than in observations, particularly in the tropics. Moreover, compared with observations, the convergence lines are relatively weak, especially over the mid-latitudes. Consequently, a smaller proportion of the simulated precipitation can be attributed to the convergence lines relative to observations, although the percentage is still high (between 55-90%). The spatial biases in the frequency of the convergence lines and the attributable precipitation are similar, although the precipitation in all the models is more strongly correlated with the associated convergence strength than in observations (Supplementary Figure 4). Presumably these biases reflect the degree to which model precipitation is triggered, organized and maintained by long-lived large-scale convergence lines. In addition, biases in the frequency and strength of

convergence lines identified in the models may simply be a result of the different native resolutions of the models compared to ERA-Interim despite regridding all data onto a common grid prior to analysis. However, there is no clear relationship between the native resolution of each model and their respective current climate biases (Supplementary Table 1). That is, models with a higher resolution (e.g. CMCC-CM) or close to ERA-Interim (e.g. CNRM-CM5, MIROC5) do not show better agreement with ERA-Interim than lower resolution models (e.g. BNU-ESM). In regions such as over small islands where shorter convergence lines occur (Weller *et al*., 2017), the MMEM underestimation may be even more exacerbated as the regridding method may turn a single convergence grid point for low resolution models (e.g. BCC-CSM1-1, BNU-ESM) into two convergence points, thus creating a convergence line over those regions.

The projections for the future greenhouse warming scenario RCP8.5 shows that the convergence line frequency and strength over the mid-latitudes weakens further, with numerous dipole patterns forming in the tropics. The large dipole frequency changes are generally associated with shifts in the major low-latitude convergence zones associated with changes in the SST gradient, consistent with prominent precipitation changes. Because of the strong relationship between convergence lines and precipitation, changes in the objectively identified organized convergence lines appear to account for most of the dynamical component in precipitation changes reported in earlier studies. Additionally, the analysis identifies where both thermodynamic and dynamics effects influence the projected precipitation changes resulting in regional precipitation changes that are different to those due to organized convergence lines alone. For example, some regions such as the western Pacific and the SPCZ exhibit a decrease in the strength of the convergence lines and little to no change in their frequency, yet show an increase in precipitation. However, the proportion of convergence lines associated with precipitation increases, highlighting that in these regions the precipitation

change may be more influenced by larger positive thermodynamic changes due to such factors as increased specific humidity.

As the models represent the low-level convergence reasonably well, this study provides an insightful measure of how the dominant dynamical component of precipitation and, more specifically, regional precipitation may change in a further warming climate. This study supports previously reported suggestions that much of the spatial pattern in projected precipitation changes arises from shifts in the major convergence zones. However, examining these precipitation-producing features on a finer temporal scale (i.e. sub-daily) further increases our understanding and confidence in the projected changes in precipitation.

The individual contributions to the precipitation changes from changes in the convergence line occurrence and changes in their strength remains to be quantified. This may be important as the models do not exhibit as high a correlation between the convergence line frequency and precipitation in the current climate, yet they show a higher correlation between their strength and precipitation. This will be addressed in a subsequent study.

Acknowledgements

The ERA-Interim data used were obtained via the ECMWF MARS website. We acknowledge the World Climate Research Programme's Working Group on Coupled Modelling, which is responsible for CMIP, and we thank the climate modelling groups for producing and making their model output available. The convergence line identification code can be made available to readers via request to the authors.

This study was supported by the Australian Research Council Centre of Excellence for Climate System Science (CE110001028).

References

Berry, G. and M. J. Reeder (2014), Objective identification of the Intertropical Convergence Zone: Climatology and trends from the ERA-Interim, *J. Clim.*, 27, 1894-1909.

Birch, C. E., J. H. Marsham, D. J. Parker, and C. M. Taylor (2014), The scale dependence and structure of convergence fields preceding the initiation of deep convection, *Geophys. Res. Lett*., 41, 4769-4776, doi:10.1002/2014GL060493.

Birch, C. E., M. Roberts, L. Garcia-Carreras, D. Ackerley, M. J. Reeder, A. Lock, and R. Schiemann (2015), Sea breeze dynamics and convection initiation: The influence of convective parameterization on model biases, *J. Clim.*, 28, 8093 – 8108.

Bony, S., G. Bellon, D. Klocke, S. Sherwood, S. Fermepin, and S. Denvil (2013), Robust direct effect of carbon dioxide on tropical circulation and regional precipitation, *Nat. Geosci*., 6, 447-451.

Bony, S., et al. (2015), Clouds, circulation and climate sensitivity, *Nat. Geosci.*, 8, 261-268.

Cai, W., et al. (2012), More extreme swings of the South Pacific convergence zone due to greenhouse warming, *Nature*, 488, 365–369.

Chadwick, R., I. Boutle, and G. Martin (2013), Spatial patterns of precipitation change in CMIP5: Why the rich do not get richer in the tropics, *J. Clim.*, 26, 3803-3822.

Chadwick, R., P. Good, T. Andrews, and G. Martin (2014), Surface warming patterns drive tropical rainfall pattern responses to CO_2 forcing on all timescales, *Geophys. Res. Lett*., 41, 610-615, doi:10.1002/2013GL058504.

Chou, C., J. D. Neelin, C.-A. Chen, and J.-Y. Tu (2009), Evaluating the ''rich-get-richer'' mechanism in tropical precipitation change under global warming, *J. Clim.*, 22, 1982–2005.

Christensen, J. H., et al. (2013), Climate Phenomena and their Relevance for Future Regional Climate Change, *In: Climate Change 2013: The Physical Science Basis. Contribution of Working Group I to the Fifth Assessment Report of the Intergovernmental Panel on Climate Change [Stocker, T. F., et al. (eds.)]*, 1217-1308, Cambridge University Press, Cambridge, United Kingdom and New York, NY, USA.

Dee, D. P., et al. (2011), The ERA-Interim reanalysis: Configuration and performance of the data assimilation system, *Q. J. R. Meteorol. Soc*., 137, 553-597.

Hastenrath, S. (1995), *Climate Dynamics of the Tropics*, 488 pp., Kluwer Acad., Norwell, Mass.

He, J., B. J. Soden, and B. Kirtman (2014), The robustness of the atmospheric circulation and precipitation response to future anthropogenic surface warming, *Geophys. Res. Lett*., 41, 2614-2622, doi:10.1002/2014GL059435.

Held, I. M., and B. J. Soden (2006), Robust responses of the hydrological cycle to global warming, *J. Clim.*, 19, 5686–5699.

Huang, P., S.-P. Xie, K. Hu, G. Huang, and R. Huang (2013), Patterns of the seasonal response of tropical rainfall to global warming, *Nat. Geosci*., 6, 357–361.

Jakob, C. (2014), Going back to basics, *Nat. Clim. Change*, 4, 1042-1045, doi:10.1038/climate2445.

Joyce, R. J., J. E. Janowiak, P. A. Arkin, and P. Xie (2004), CMORPH: A method that produces global precipitation estimates from passive microwave and infrared data at high spatial and temporal resolution, *J. Hydrometeor.*, 5, 487-503.

Kent, C., R. Chadwick, and D. P. Rowell (2015), Understanding uncertainties in future projections of seasonal tropical precipitation, *J. Clim.*, 28, 4390–4413.

Kjellsson, J. (2015), Weakening of the global atmospheric circulation with global warming, *Clim. Dyn*., 45, 975-988, doi:10.1007/s00382-014-2337-8.

Lu, J., G. A. Vecchi, and T. Reichler (2007), Expansion of the Hadley cell under global warming, *Geophys. Res. Lett*., 34, L06805, doi:10.1029/2006GL028443.

Neelin, J., C. Chou, and H. Su (2003), Tropical drought regions in global warming and El Niño teleconnections, *Geophys. Res. Lett.*, 30, doi: 10.1029/2003GL018625.

Reeder, M. J., et al. (2013), Diurnally forced convergence lines in the Australian tropics, *Quart. J. R. Meteor. Soc.*, 139, 1283-1297.

Rybka, H., and H. Tost (2014), Uncertainties in future climate predictions due to convection parameterisation, *Atmos. Chem. Phys.*, 14, 5561-5576.

Scheff, J., and D. Frierson (2012), Twenty-first-century multimodel subtropical precipitation declines are mostly midlatitude shifts, *J. Clim.*, 25, 4330–4347.

Seager, R., N. Naik, and G. A. Vecchi (2010), Thermodynamic and dynamic mechanisms for large-scale changes in the hydrological cycle in response to global warming, *J. Clim.*, 23, 4651–4668.

Shepherd, T. G. (2014), Atmospheric circulation as a source of uncertainty in climate model projections, *Nat. Geosci*., 7, 703–708.

Stephens, G. L., et al. (2010), Dreary state of precipitation in global models, *J. Geophys. Res.*, 115, D24211, doi:10.1029/2010JD014532.

Taylor, K. E., Stouffer, R. J., and Meehl, G. A. (2012), An overview of CMIP5 and the experiment design, *Bull. Amer. Meteor. Soc.*, 93, 485-98.

Vecchi, G. A., and B. J. Soden (2007), Global warming and the weakening of the tropical circulation, *J. Clim*., 20, 4316–4340.

Weller, E., K. Shelton, M. J. Reeder, and C. Jakob (2017), Precipitation associated with convergence lines, *J. Clim*., 30, 3169-3183.

Widlansky, M. J., P. J. Webster, and C. D. Hoyos (2010), On the location and orientation of the South Pacific Convergence Zone, *Clim. Dyn*., 36, 561-578., doi:10.1007/s00382-010-0871-6.

Widlansky, M. J., et al. (2013), Changes in South Pacific rainfall bands in a warming climate, *Nat. Clim. Change*, 3, 417-423, doi:10.1038/nclimate1726.

Wills, R. C., M. P. Byrne, and T. Schneider (2016), Thermodynamic and dynamical controls on changes in the zonally anomalous hydrological cycle, *Geophys. Res. Lett*., 43, 4640-4649, doi:10.1002/2016GL068418.

Wodzicki, K. R., and A. D. Rapp (2016), Long-term characterization of the Pacific ITCZ using TRMM, GPCP, and ERA-Interim, *J. Geophys. Res. Atmos.*, 121, 3153–3170.

Xie, S.-P., C. Deser, G. A. Vecchi, J. Ma, H. Teng, and A. T. Wittenberg (2010), Global warming pattern formation: Sea surface temperature and rainfall, *J. Clim.*, *23*(4), 966–986.

Figure Caption List

Figure 1. Annual-means of convergence line frequency (proportion of month (% month^{-1})) for (a) ERA-Interim, (b) multimodel mean Historical simulations, and (c) multimodel mean bias (models minus ERA-Interim) over the period 1979-2005. (d)-(f) Same as (a)-(c) respectively, but for the convergence line strength (s^{-1} scaled by 10^5).

Figure 2. Annual-means of convergence line frequency (proportion of month (% month^{-1})) for (a) multimodel mean RCP8.5 simulations (2080-2100), and (b) multimodel mean change (RCP8.5 2080-2100 minus Historical 1979-2005). (c)-(d) Same as (a)-(b) respectively, but for the convergence line strength (s^{-1} scaled by 10^5).

Figure 3. Zonal mean seasonal cycle of the convergence line frequency (proportion of month (% month^{-1})) for (a) ERA-Interim (1979-2005), (b) multimodel mean Historical simulations (1979-2005), and (c) multimodel mean change (RCP8.5 2080-2100 minus Historical 1979-2005). In (a) and (b) respectively, the solid curve marks the latitude of the maximum in the precipitation climatology from CMORPH and multimodel mean Historical climate. In (c), the solid (dashed) curve marks the latitude of the maximum convergence line frequency in the multimodel (ERA-Interim) Historical climate.

Figure 4. Multimodel mean changes (RCP8.5 2080-2100 minus Historical 1979-2005) in (a) total precipitation (shaded, mm day^{-1}) and relative SST (to the tropical (20°S to 20°N) mean warming; contours at intervals of 0.25°C; negative dashed), (b) proportion of precipitation (%) associated with objectively identified convergence lines, and the frequency of convergence lines (proportion of month (% $month^{-1}$)) (c) not associated with precipitation (dry lines) and (d) associated with precipitation (wet lines). Note the color scale in Figure 4 is opposite to that for the other figures so that red is used to denote a decrease in precipitation, and blue an increase.

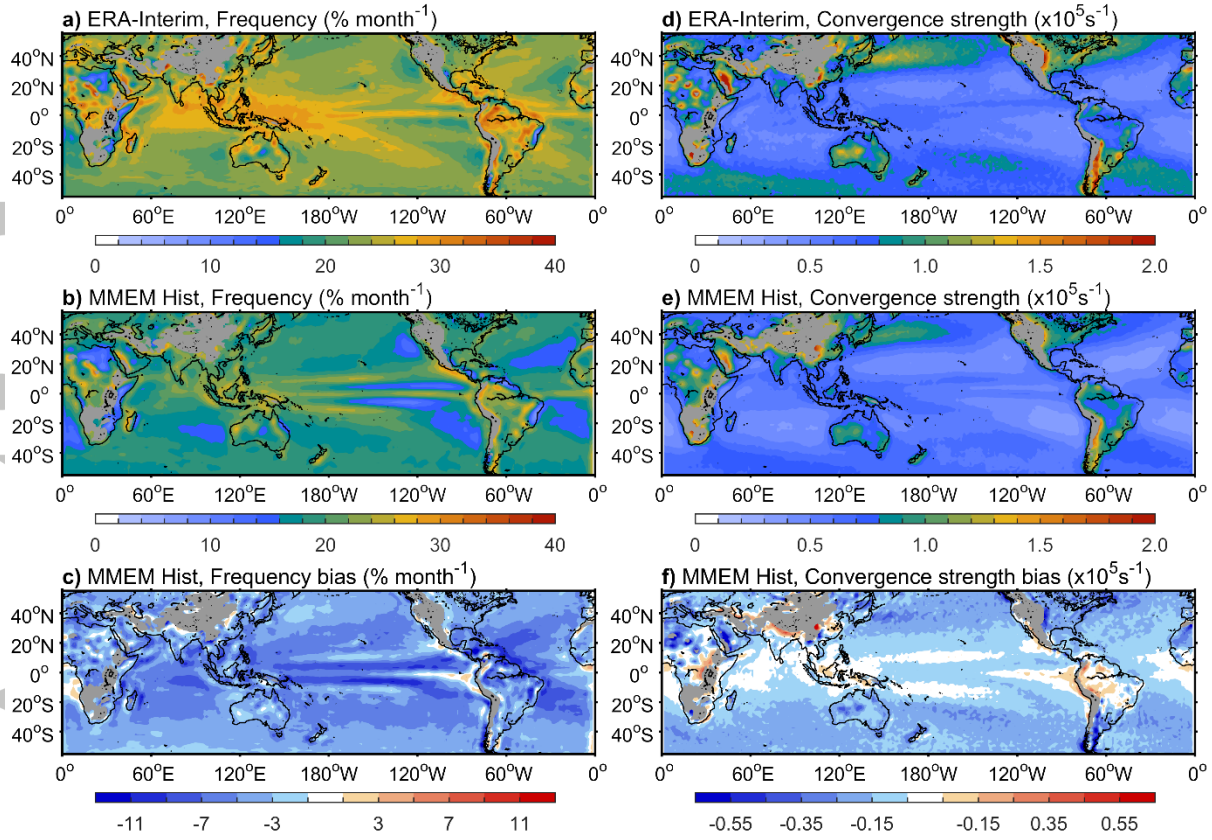

Figure 1. Annual-means of convergence line frequency (proportion of month (% month^{-1})) for (a) ERA-Interim, (b) multimodel mean Historical simulations, and (c) multimodel mean bias (models minus ERA-Interim) over the period 1979-2005. (d)-(f) Same as (a)-(c) respectively, but for the convergence line strength (s^{-1} scaled by 10^5).

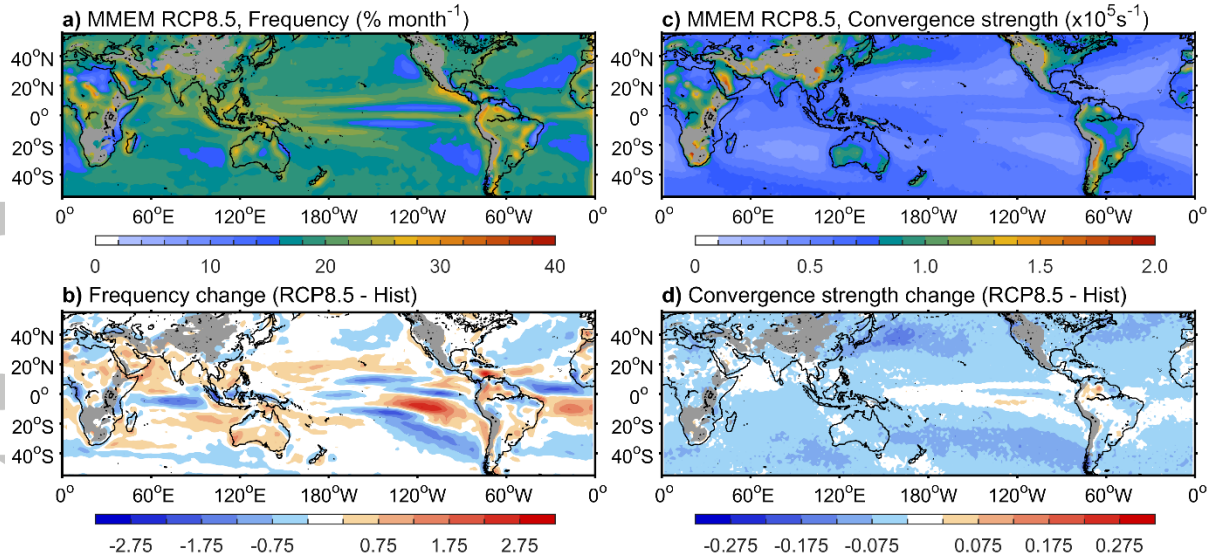

Figure 2. Annual-means of convergence line frequency (proportion of month (% month^{-1})) for (a) multimodel mean RCP8.5 simulations (2080-2100), and (b) multimodel mean change (RCP8.5 2080-2100 minus Historical 1979-2005). (c)-(d) Same as (a)-(b) respectively, but for the convergence line strength (s^{-1} scaled by 10^5).

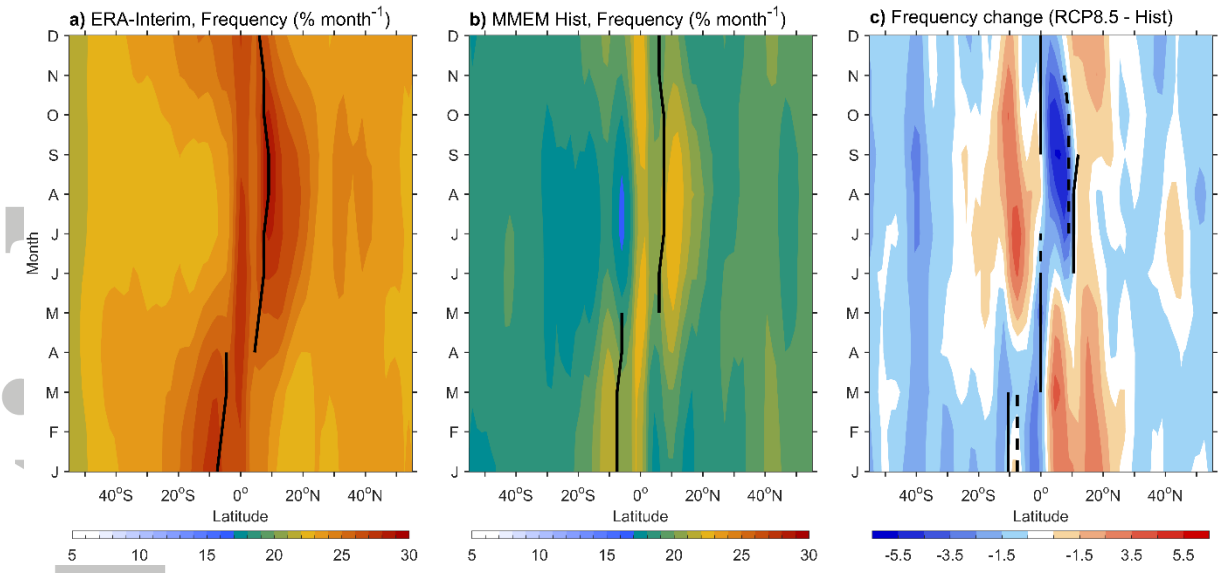

Figure 3. Zonal mean seasonal cycle of the convergence line frequency (proportion of month (% month^{-1})) for (a) ERA-Interim (1979-2005), (b) multimodel mean Historical simulations (1979-2005), and (c) multimodel mean change (RCP8.5 2080-2100 minus Historical 1979-2005). In (a) and (b) respectively, the solid curve marks the latitude of the maximum in the precipitation climatology from CMORPH and multimodel mean Historical climate. In (c), the solid (dashed) curve marks the latitude of the maximum convergence line frequency in the multimodel (ERA-Interim) Historical climate.

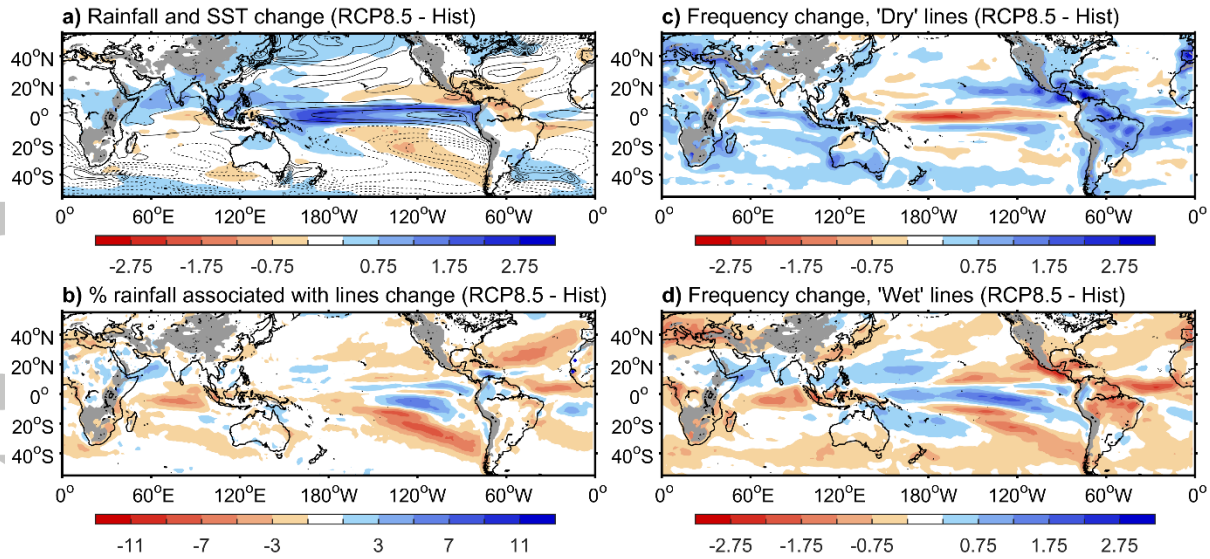

Figure 4. Multimodel mean changes (RCP8.5 2080-2100 minus Historical 1979-2005) in (a) total precipitation (shaded, mm day^{-1}) and relative SST (to the tropical (20°S to 20°N) mean warming; contours at intervals of 0.25°C; negative dashed), (b) proportion of precipitation (%) associated with objectively identified convergence lines, and the frequency of convergence lines (proportion of month (% month^{-1})) (c) not associated with precipitation (dry lines) and (d) associated with precipitation (wet lines). Note the color scale in Figure 4 is opposite to that for the other figures so that red is used to denote a decrease in precipitation, and blue an increase.